Influence area on the end bearing capacity of a pile in three-dimensional analysis under various soil conditions

Junichi Hyodo, Kyohei Sato & Yukio Tamari
Tokyo Electric Power Services Co. Ltd, Koto, Tokyo, Japan
Osamu Ozutsumi
Meisosha Corporation, Toshima, Tokyo, Japan
Koji Ichii
Hiroshima University, Higashi-hiroshima, Hiroshima, Japan

ABSTRACT

Most of the piles supporting tall buildings reach rigid base. However, there are some cases where some piles accidentally did not reach the firm base. However, from the viewpoint of performance-based seismic design, it is not necessary to rebuild all buildings in such condition. If the number of unreached pile is limited, or if the unreached distance to the rigid base is limited, a certain level of bearing capacity may be expected. Thus, the cost and benefit analysis for the rebuild the buildings shall be done in the performance-based design concept.

For the accurate estimation of the inclination of these building with unreached pile, adequate modeling of unreached piles is necessary. In addition, the seismic performance of the unreached pile may be dependent on the balance of the unreached distance and the influence area around pile tip. In this study, we examine the influence area of soils around the pile bottom as a function of the soil condition. This summary can provide fundamental background on the application of various techniques to model the unreached pile to the rigid base.

1 INTRODUCTION

Most of the piles supporting tall buildings reach rigid base. However, there are some cases where some piles accidentally did not reach the firm base. Expected bearing capacity is not sufficient in such cases, and rebuild of the building shall be discussed.

However, from the viewpoint of performance-based seismic design, it is not necessary to rebuild all buildings in such condition. If the number of unreached pile is limited, or if the unreached distance to the rigid base is limited, a certain level of bearing capacity may be expected. For example, Figure 1 shows an example of the FEM analysis of a building with unreached pile to the rigid base. Since the left pile did not reached to the rigid base (distance is 0.1D), the building inclined toward the left side after earthquake. However, if this inclination is permissible and there is no collapse of the building, rebuild is not necessary. Thus, the cost and benefit analysis for the rebuild of the buildings shall be done in the performance-based design concept.

For the accurate estimation of the inclination of these building with unreached pile, adequate modeling of unreached piles is necessary. Thus, appropriate model of pile tip in practical analysis is important. In addition, the performance of the unreached pile may be dependent on the balance of the unreached distance and the influence area around pile tip. Thus, a detailed discussion on influence area around pile tip where deformation of the soil may occur is also a quite important issue.

In this study, we introduce several type of pile model in 2D analysis, and we emphasize the importance of influence area. Then, with a sophisticated 3D analysis, we examined the influence area of soils around the pile bottom as a function of the soil condition.

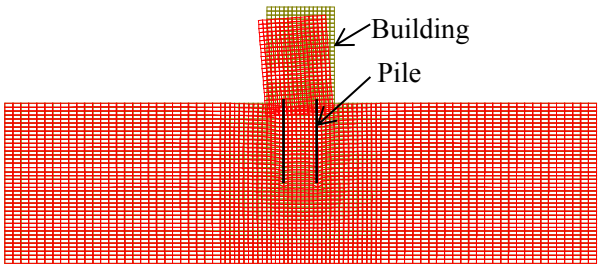

Figure 1 Example of FEM analysis of a building with unreached pile during earthquake loading

2 MODELING OF THE PILE-TIP IN 2D ANALYSIS

2.1 Various type of the model for pile tip

We assumed four models, A – D, which were used to research the pile-soil interaction at the pile end in the vertical direction. All models indicate a subgrade reaction in the horizontal direction due to the pile-soil interaction elements. Model A models the subgrade reaction in the horizontal direction by a pile-soil interaction element and the end bearing capacity of the pile by same displacement between the pile tip and the ground. In Models B – D, the

end bearing capacity of a pile is modeled by a nonlinear spring element. The nonlinear spring element is set in series between the pile tip and the ground. In Model B, the ground nodal point is fixed. In Model D, the ground nodal point is a multi-point constraint bound by the influence area for the end bearing capacity.

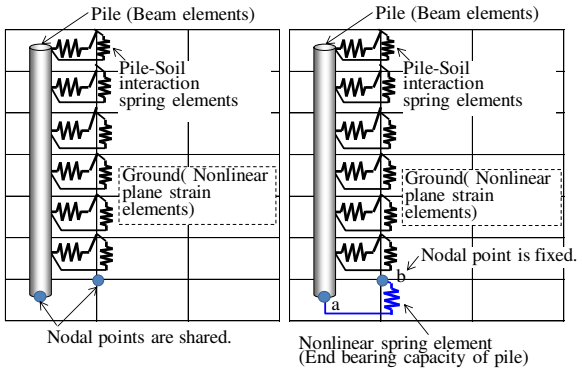

(a) Model A (b) Model B

Figure 1. Models for the pile-soil interaction in the 2D analysis

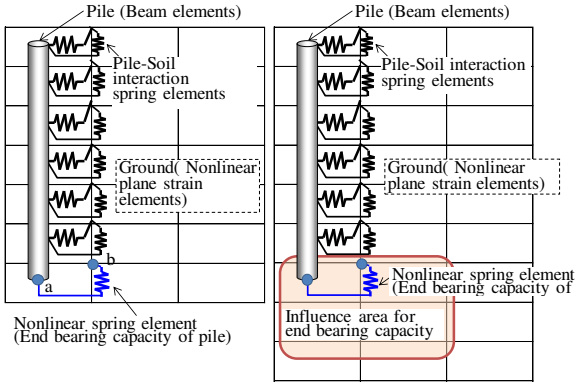

(a) Model C (b) Model D

Figure 2. Model for the pile-soil interaction in the 2D analysis

2.2 2D analysis

2.2.1 Analysis conditions

We conducted 2D analysis to examine the characteristics of each model. The 2D analysis program in the FLIP series (Iai et al. (1992)), FLIP ROSE Ver7.1.9-6-2, was used. Figure 3 shows the 2D mesh used in the analysis. The ground consisted of two layers. The relative density of the upper layer was 40%, while that of the lower layer was 90%. The analysis assumed fully drained conditions. The 2D multi-spring elements with Mohr-Coulomb criteria were used for soils. The pile was modeled by linear beam elements. The bottom boundary and the lateral boundary in the x-direction were fixed. The end bearing capacity of pile was modeled using nonlinear spring elements. Specifically, we used the nonlinear spring elements proposed by Hirayama (1990). The pile penetration was given as the enforced displacement at the pile head nodes.

The soil parameters were determined by the simplified parameter setting procedures for FLIP ROSE (revised version). The parameter setting procedure was based on the SPT N-value (the N-value for effective overburden stress of 65 kPa following the design standards for Japanese ports). Tables 1, 2 and 3 show the soil, pile parameters and parameters for the nonlinear spring element, respectively.

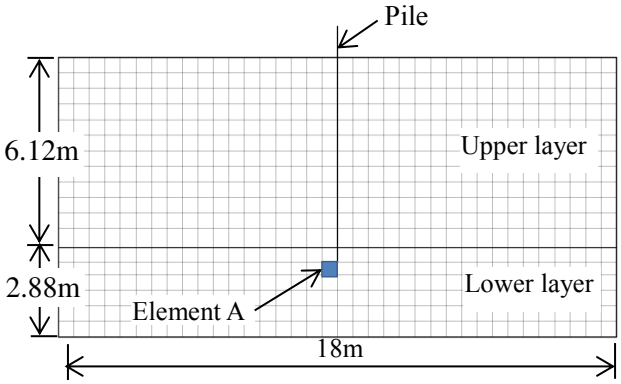

Figure 3. 2D mesh model for the analysis

Table 1. Soil parameters

Characteristics	Upper layer	Lower layer
Relative density Dr (%)	60	90
Wet density ρ (t/m^3)	1.93	1.99
Shear modulus G_{ma} (kPa)	8.97×10^4	1.51×10^5
Bulk modulus K_{ma} (kPa)	2.34×10^5	3.94×10^5
Reference confining effective stress σ'_{ma} (kPa)	98.0	98.0
Reference parameter m_G, m_K	0.5	0.5
Cohesion C (kPa)	0.0	0.0
Internal friction angle ϕ (degrees)	39.86	42.05

Table 2. Pile parameters

Diameter (m)	0.48
Thickness (m)	0.032
Young's modulus (kPa)	1.05×10^9
Poisson's ration	0.35
Area (m^2)	0.045
Second moment of area (m^4)	1.14×10^{-3}

Hirayama (1990) proposed a hyperbolic correlation between the pile end resistance and the pile tip displacement, as shown in Fig. 4 and Eq. 1. Hirayama

reported that the hyperbolic correlation is consistent with the results of the in situ test. Furthermore, there are only two parameters in the hyperbolic correlation, making it suitable for practical use. Thus, we used the hyperbolic correlation as a nonlinear spring element between the pile tip and the ground.

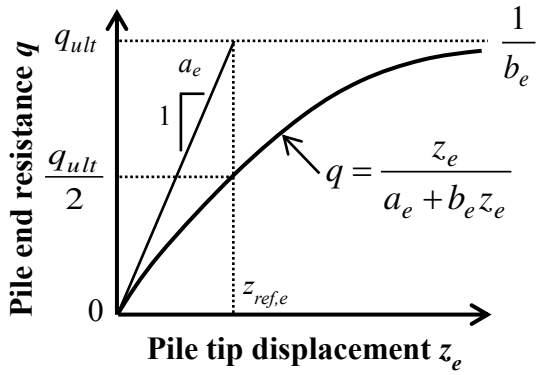

Figure 4. Relationship between the pile tip displacement and the pile end resistance (Hiarayama (1990))

Table 3. Parameters for the nonlinear spring element

$q_{0.1}$ (kN/m^2)	2625
a_e (m/(kN/m^2))	1.31x10^{-5}
b_e (1/(kN/m^2))	1.09x10^{-4}
q_{ult} (kN/m^2)	9178
Area A (m^2)	0.181
$q_{0.1}$ A (kN)	475
q_{ult} A (kN)	1661

$$q = \frac{z_e}{a_e + b_e z_e} \quad [1]$$

$$a_e = \frac{z_{ref,e}}{q_{ult}} = \frac{0.25 D_e}{q_{ult}}, \quad b_e = \frac{1}{q_{ult}} \quad [2]$$

Parameters a_e and b_e are given by Eq. 2. A reference displacement $z_{ref,e} = 0.25D_e$ (m) in Eq. 2 is given for sandy soil. D_e is the pile diameter, and q_{ult} is the ultimate value in the pile end resistance. It is difficult to calculate the maximum value of the pile end resistance q_{ult}. It is often the case that the Japanese design code (e.g., the AIJ standards for Design of Building Foundation) defines the end bearing capacity of a pile as the pile end resistance at 0.1 D_e.

Eq. 1 for the pile tip settlement of $z_e = 0.1\ D_e$ (m) gives

$$q_{0.1} = \frac{0.1 D_e}{a_e + b_e \cdot 0.1 D_e} \quad [3]$$

Eq. 2 and Eq. 3 give

$$q_{0.1} = 0.286 q_{ult} \quad [4]$$

Then Eq. 2 and Eq. 4 give the following equations for parameters a_e and b_e.

$$a_e = \frac{0.0715 D_e}{q_{0.1}}, \quad b_e = \frac{0.286}{q_{0.1}} \quad [5]$$

2.2.2 Analysis results

Figure 5 shows the effect of the mesh size in Model A. At a mesh size of 0.5 m or 0.25 m, the analysis results are inconsistent with the target. In Model A, the pile end resistance depends on the mesh size. Here, the anti-plane width (mesh size in the out-of-plane direction) was set as 6 m.

Figure 6 shows the effect of the anti-plane width (scale of the mesh size in the out-of-plane direction) in Model A with an in-plane mesh size 0.5 m. The analysis results depend on the mesh size in the out-of-plane direction. The pile end resistances at anti-plane widths of 6 m and 3 m are overestimated because the ground stiffness is sufficiently large. However, the pile end resistance at an anti-plane width of 1 m is approximately the same as the target, but the pile end resistance at an anti-plane width of 0.5 m is underestimated. These results demonstrate that the pile end resistance in 2D analysis depends on the mesh size in both the in-plane and the out-of-plane directions.

Figure 7 shows the relationship between the pile end resistance and the pile head displacement in Model B. The target is Hirayama's hyperbolic approximation. The results agree well with the target because the pile tip is connected to a fixed point by the nonlinear spring element. However, the vertical force at the pile tip does not act on the ground because the nodal point of nonlinear spring element at the pile tip is fixed. Therefore, the pile load does not influence the ground around the pile tip.

Figure 8 shows the relationship between the pile end resistance and the pile head displacement in Model C. The target is Hirayama's hyperbolic approximation. The analysis results basically agree with the target at anti-plane widths of 6 m and 3 m because the ground stiffness is sufficiently large. However, the analysis results at anti-plane widths of 1 m and 0.5 m are underestimated. Similar to Model A, the anti-plane width and mesh size influence the pile end resistance in Model C.

Figure 9 and Figure 10 show the effective stress pass at the ground element below the pile tip, and the compression shear stress strain relationship at the ground element below the pile tip, respectively. In Model B, the stress state of the soil element remains in the initial state. However, in Models A and C, both the mean effective stress and the maximum shear stress increase with pile

loading. In Model C, the stress remains at a steady point after reaching the maximum bearing capacity of the nonlinear spring element. In Model A, the increase in the stresses continues after reaching the maximum bearing capacity as the compression shear increases (Figure 10).

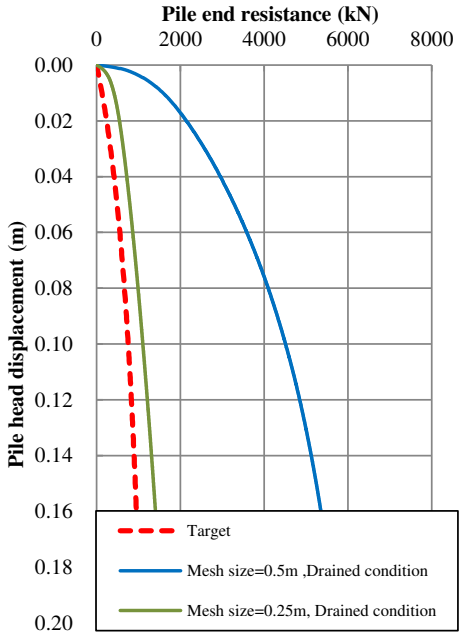

Figure 5. Relationship between the pile end resistance and the pile head displacement in Model A

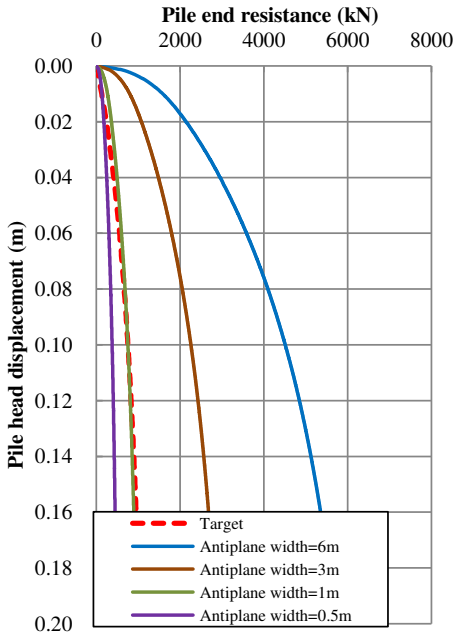

Figure 6. Relationship between the pile end resistance and the pile head displacement in Model A

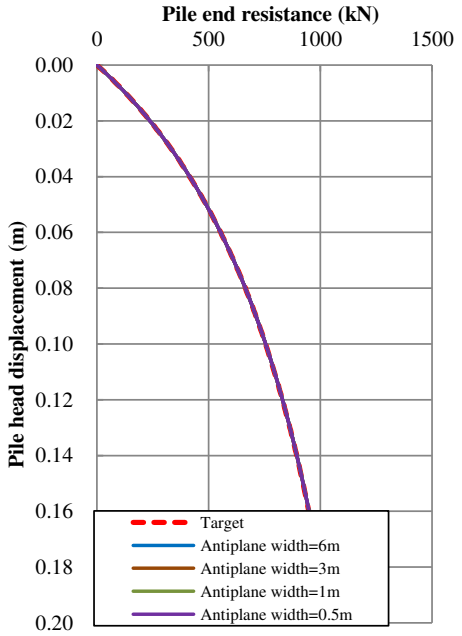

Figure 7. Relationship between the pile end resistance and the pile head displacement in Model B

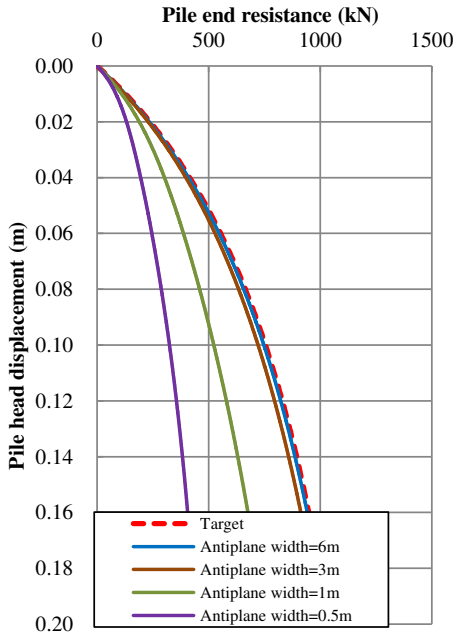

Figure 8. Relationship between the pile end resistance and the pile head displacement in Model C

Table 4. Models for the pile-soil interaction

	Model A	Model B	Model C	New model D
Concept	Pile and soil at the pile tip have the same displacement.	Pile end resistance is modeled by the nonlinear spring element. Soil nodal point in the nonlinear spring elements is fixed.	Pile end resistance is modeled by the nonlinear spring element.	Pile end resistance is modeled by the nonlinear spring elements.
Pile end resistance	Pile end resistance does not agree with the target.	Pile end resistance agrees well with the target.	Pile end resistance agrees well with the target.	Pile end resistance agrees with the target.
Problem	Pile end resistance depends on the mesh size and the anti–plane width.	The ground around pile tip is not influenced by the pile load.	It is possible to double count the ground deformation.	It is difficult to verify the area constraining the ground nodes.

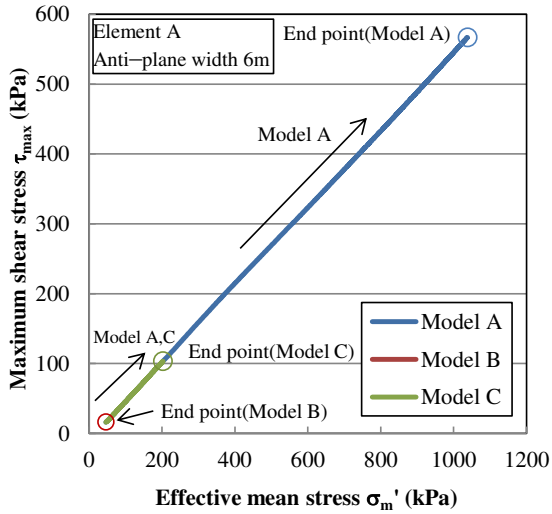

Figure 9. Effective stress path at the ground element below the pile tip

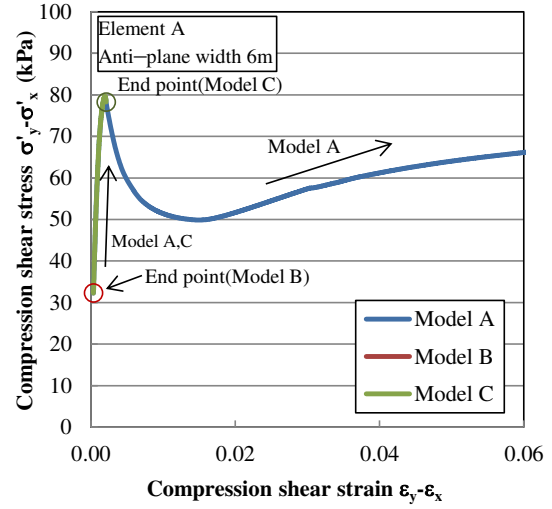

Figure 10. Compression shear stress strain relationship at the ground element below the pile tip

2.2.3 New Model D

Model C connects the nonlinear spring element and the pile tip ground in series. Model C is basically the most advanced method to simulate the pile settlement. However, it is possible to double count the ground deformation. To minimize double counting, we propose Model D, where some of the ground nodal points are constrained to have the same deformation. We conducted three-dimensional (3D) analysis because it is important in Model D that the influence area is adequately sized.

3 3D ANALYSIS

3.1 Analysis condition

For the aforementioned model, 3D analysis was performed using an analysis model (12–m high, 18–m long and 6–m width). A quarter (1/4) of all targets were modeled to save computational time, as shown in Fig. 11. The pile penetration was given as the enforced displacement at the pile head. The x-, y-, and z-axes were the length, the width, and the vertical axis, respectively. The model consisted of saturated sand in two layers (upper layer Dr=60%). The 3D analysis program in the FLIP ROSE series, FLIP (3D version) Ver1.6.2, and fully drained conditions were used. The soil parameters are shown in Table 5 and Fig. 12, while Table 2 shows the pile parameters.

The 3D multi-spring model elements with the Mohr-Coulomb's failure criteria for the soil were used. The shell elements were used for the pile. Joint elements were inserted between the soil and the pile. All the nodes at the pile tip and the ground in contact with the pile tip were combined to have the same movement in the z-direction. Roller boundary conditions were applied to the side boundaries (xz-plane and yz-plane), while the bottom boundary was fixed. On the symmetrical plane (y=0), movement in the y-direction and rotational movement around the x-axis and z-axis were fixed. To focus on the end bearing capacity of the pile, the pile-soil friction at the joint elements was set to zero. Thus, the bearing capacity at the pile head and that at the pile tip are the same.

Table 5. Model for the pile-soil interaction

Characteristics	Lower layer Case1	Lower layer Case2	Lower layer Case3
Relative density Dr (%)	45	60	90
Wet density ρ (t/m^3)	1.99	1.99	1.99
Shear modulus G_{ma} (kPa)	6.33×10^4	8.97×10^4	1.51×10^5
Bulk modulus K_{ma} (kPa)	1.65×10^5	2.34×10^5	3.94×10^5
Reference confining effective stress σ'_{ma} (kPa)	98.0	98.0	98.0
Reference parameter m_G, m_K	0.5	0.5	0.5
Cohesion C (kPa)	0.0	0.0	0.0
Internal friction angle ϕ (degrees)	30,35,40,45	30,35,40,45	30,35,40,45

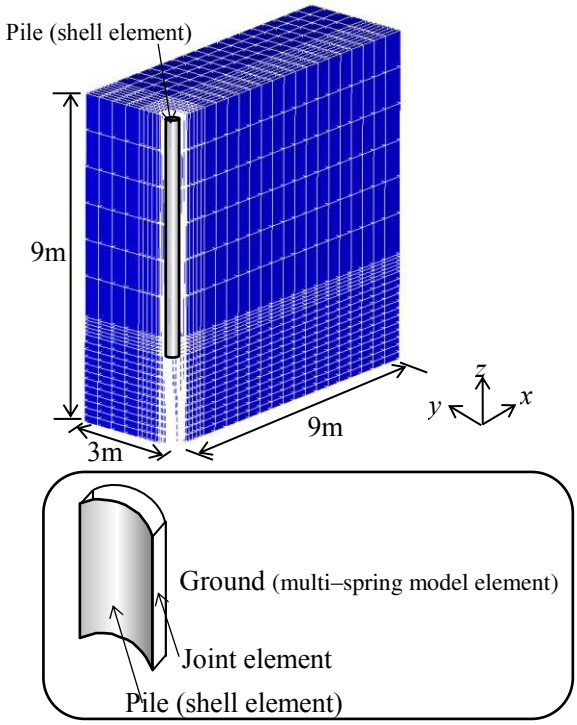

Figure 11. 3D model for the analysis

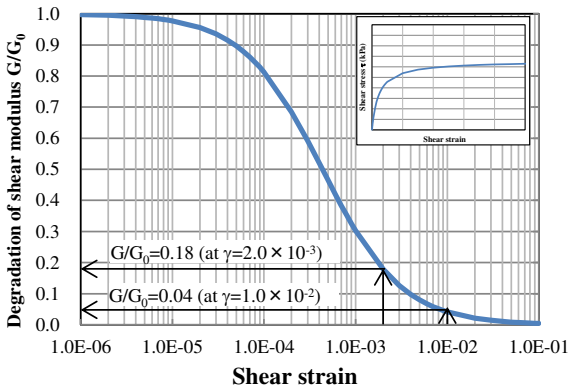

Figure 12. Degradation of the shear modulus in the lower layer (from the hyperbolic relationship)

3.2 Analysis results

Figure 13 shows the relationship between the pile end resistance $q_{0.1}$ at the settlement of 10% of the pile diameter and the internal friction angle of lower layer. The pile end resistance increases with the internal friction angle. Figure 14 shows the relationship between the pile end resistance and the pile head displacement. The pile end resistance increases with the internal friction angle.

Figure 15 shows the ground deformation at a settlement of 10% of the pile diameter with the distribution of the effective vertical stress σ_z' and the maximum shear strain γ_{max} in Case 3 (Dr=90%). The shape of the pressure bulb is observed as a region of high vertical stress and large strain. In this case, the area of high stress and strain is approximately 2 to 3 times the pile diameter in both the vertical and horizontal directions.

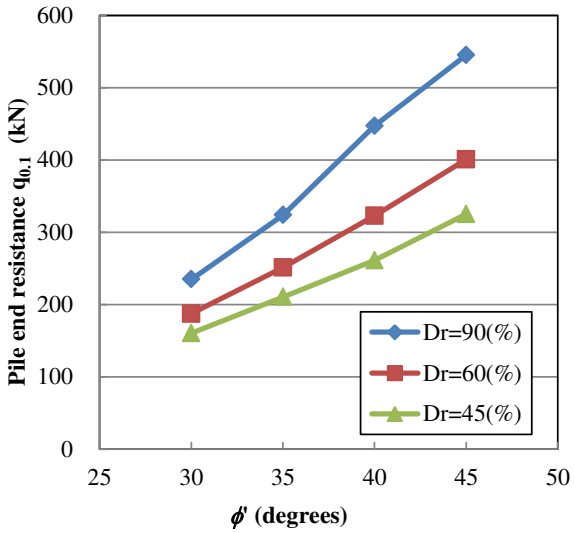

Figure 13. Pile end resistance $q_{0.1}$ at the settlement of 10% of the pile diameter

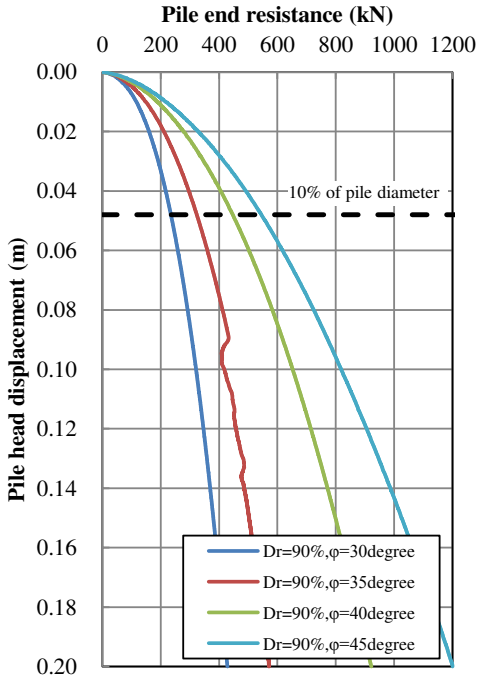

Figure 14. Relationship between the pile end resistance and the pile head displacement in 3D analysis

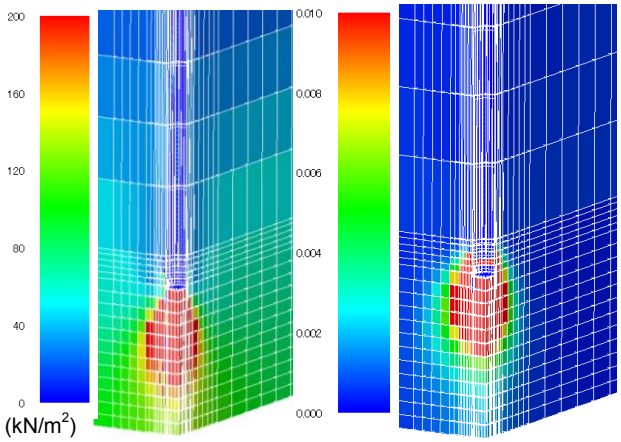

(a) Vertical effective stress (b) Maximum shear strain

Figure 15. Deformation (at settlement of 10% of the pile diameter), the vertical effective stress, and the maximum shear strain in the 3D analysis (Dr=90%, ϕ=40 degrees)

4 INFLUENCE AREA ON THE END BEARING CAPACITY OF A PILE

Yang (2006) proposed the influence area for the end bearing capacity of a pile using the spherical cavity expansion theory. Figure 16, Eq. 6, and Eq. 7 show the influence area below the pile tip proposed by Yang (2006).

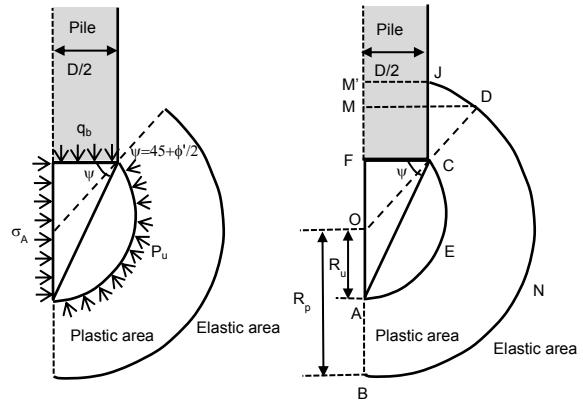

Figure 16. Influence area for piles below the pile tip (Yang (2006))

$$\left(\frac{I_{FD}}{D}\right)=\frac{1}{2}\left(\tan\phi'+\frac{\zeta}{\cos\phi'}\right) \quad [6]$$

$$\left(\frac{I_{FD}}{D}\right)=\left(\frac{FB}{D}\right)=\frac{1}{2}\left(tan\phi'+\sqrt{\frac{G}{G\Delta+p_0'\tan\phi'}}\cdot\frac{1}{cos\,\phi'}\right) \quad [7]$$

Here ϕ' is the effective internal friction angle of the sand beneath the pile. G is the shear modulus, p_0' is the effective confining pressure, and Δ is the average volumetric strain in the plastic zone. ζ is R_p/R_u. Yasufuku et al. (2001) suggested an empirical relationship for the average volumetric strain for sands varying from stiff sand to compressible sand.

$$\Delta=50(I_r)^{-1.8} \quad [8]$$

$$I_r=\frac{G}{p_0'\tan\phi'} \quad [9]$$

where I_r is rigidity index.

In this study, we defined the influence for the end bearing capacity of the pile area as the large shear strain area at a settlement of 10% in the 3D analysis. Figure 17 and Figure 18 show the influence area for piles below the pile tip at maximum shear strains γ_{max}=0.001 and γ_{max}=0.01 in the 3D analysis, respectively. The solid lines show the influence area proposed by Yang (2006). Degradation of the shear modulus (G/G_0) at maximum shear strains γ_{max}=0.001 and γ_{max}=0.01 are G/G_0=0.18 and G/G_0=0.04, respectively.

The influence area on the end bearing capacity of a pile in 3D analysis is approximately the same as that of Yang's method. The influence area in the 3D analysis is slightly influenced by the internal friction angle and the shear modulus at maximum shear strain γ_{max}=0.002. However, the shear modulus at a maximum shear strain γ_{max}=0.01 does not impact the influence area in 3D analysis.

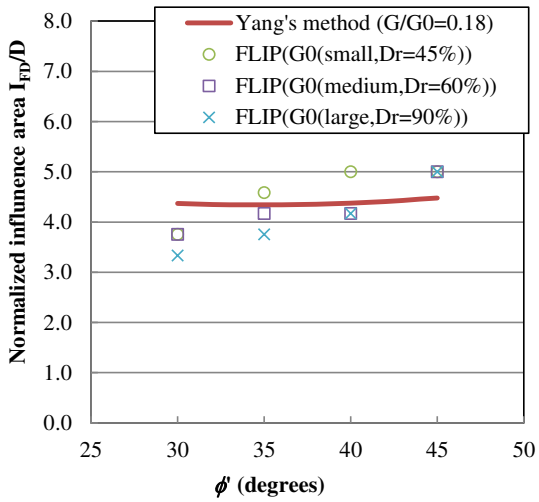

Figure 17. Influence area for piles below the pile tip at settlement of 10% of the pile diameter and a maximum shear strain γ_{max}=0.002

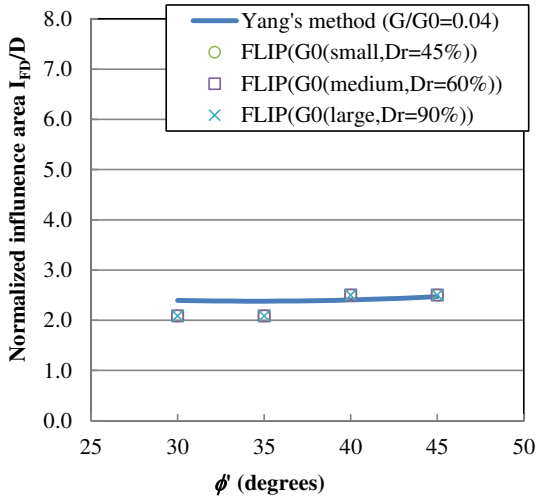

Figure 18. Influence area for piles below the pile tip at settlement of 10% of the pile diameter and a maximum shear strain γ_{max}=0.01

5 CASE STUDY FOR NEW MODEL D

5.1 Analysis conditions

We conducted 2D effective stress analysis to examine the applicability on new model D. The 2D analysis program in the FLIP series was used. Figure 19 shows the 2D mesh used in the analysis (Tobita et al. (2015)). The ground consists of two layers. The upper layer is liquefied layer. The analysis assumed undrained conditions. The 2D multi-spring elements with Mohr-Coulomb criteria were used for soils. The pile was modeled by the linear beam elements. The end bearing capacity of pile was modeled using spring elements. The New Model D(Figure 2(b)) for the pile-soil interaction was used. To consider the influence area on the end bearing capacity of a pile, the ground nodal point was a multi-point constraint. Table 6, 7 and 8 show the soil parameters, parameters for the nonlinear spring element and analysis cases, respectively. Figure 20 shows the input motion.

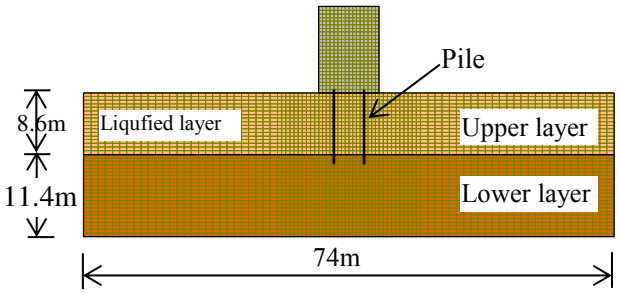

Figure 19. 2D mesh model for the analysis

Table 6. Soil parameters

Characteristics	Upper layer	Lower layer
Wet density ρ (t/m^3)	1.85	1.94
Shear modulus G_{ma} (kPa)	5.57×10^4	1.75×10^5
Bulk modulus K_{ma} (kPa)	1.45×10^5	4.56×10^5
Reference confining effective stress σ'_{ma} (kPa)	98.0	98.0
Reference parameter m_G, m_K	0.5	0.5
Cohesion C (kPa)	0.0	0.0
Internal friction angle ϕ (degrees)	38.48	43.00
Phase transformation angle ϕ_p(degrees)	28.0	-
S_1	0.005	-
w_1	9.45	-
p_1	0.50	-
p_2	0.50	-
c_1	1.00	-

Table 7. Parameters for the nonlinear spring element

N-value	50	20
$q_{0.1}$ (kN/m^2)	15000	6000
a_e (m/(kN/m^2))	$5.72\text{x}10^{-6}$	$1.43\text{x}10^{-5}$
b_e (1/(kN/m^2))	$1.91\text{x}10^{-5}$	$4.77\text{x}10^{-5}$
Area A (m^2)	1.13	1.13
$q_{0.1}$ A (kN)	17000	6790

Table 8. Analysis cases

End bearing capacity of a pile	Case1	Case2
N-value of left pile	50	20
N-value of right pile	50	50

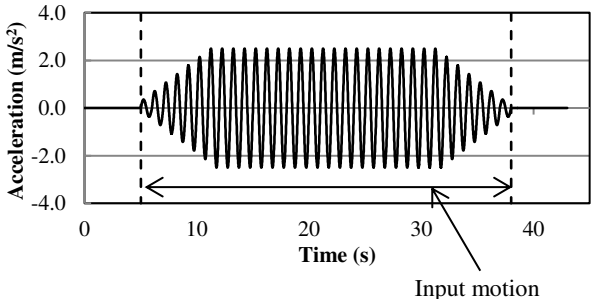

Figure 20. Input motion

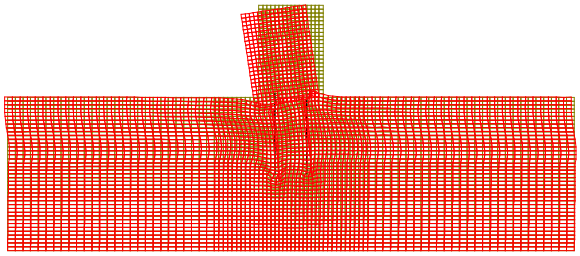

Figure 21. Deformation at 12.942 (s) (Case2)

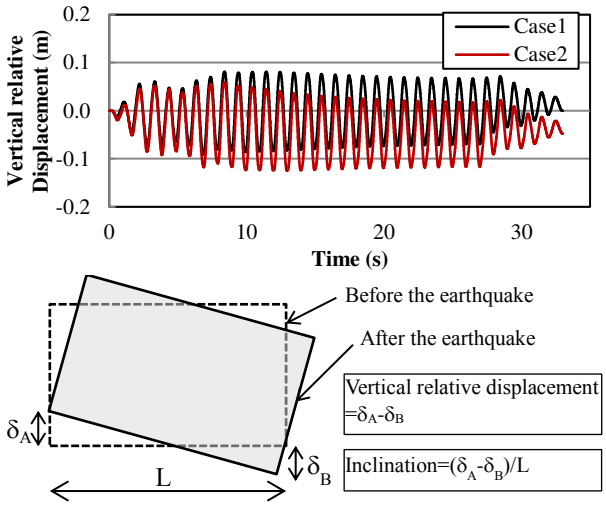

Figure 22. Vertical relative displacement of the building

5.2 Analysis results

Figure 21 shows the deformation at 12.942(s). Figure 22 shows the vertical relative displacement. The vertical displacement in Case2 is larger than that in Case1. This is because the left pile in Case2 is unreached pile. It is possible that New Model D in 2D analysis is applicable to examine the performance of the building with unreached pile.

6 CONCLUSIONS

We conducted 3D analysis to examine the influence area on the end bearing capacity of a pile. We considered the shear modulus and the internal friction angle as parameters.

The influence area at a settlement of 10% of the pile diameter in the 3D analysis is approximately the same as that of Yang's method. The influence area in the 3D analysis is slightly affected by the internal friction angle. Additionally, the influence area is impacted by the shear modulus at a maximum shear strain γ_{max}=0.002, but not by the shear modulus at a maximum shear strain γ_{max}=0.01.

In the practical seismic design process, 2D analysis is often used. We would like to verify the 2D simple model (Model D) for the pile bottom using the abovementioned influence area.

In the future, we would like to propose a method to estimate the reduction of seismic performance of the structure with unreached piles. For example, if the unreached distance is more than the height of influence area, the end bearing capacity of these piles shall be reduced a certain level.

ACKNOWLEDGEMENT

This research were supported by the discussion in a WG in FLIP Consortium. The authors sincerely appreciated the contributions and supports by WG member.

REFERENCES

Iai, S., Matsunaga, Y., Kameoka, T. 1992. Strain space plasticity model for cyclic mobility, *Soils and Foundations*, Vol.32, No.2, pp.1-15.

Hirayama, H. 1990. Load-settlement analysis for bored piles using hyperbolic transfer functions, *Soils and Foundations*, Vol.30 , No.1:55-64.

Yang, J. 2006. Influence zone for end bearing of piles in sand, *Journal of geotechnical and geoenvironmental engineering*:1229-1237.

Yasufuku, N., Ochiai, H. and Ohno, S. 2001. Pile end-bearing capacity of sand related to soil compressibility, *Soils and foundations*, Vol.41, No.4:59-71.

Tobita, T., Iai, S. and Ouchi, S. 2015. Combined failure mechanism of a building supported by piled foundations under liquefaction and tsunami, *Journal of Natural Disaster Science*, Vol.34, No.1, pp23-39. (In Japanese)